

3D printing for heat transfer: characterisation of additive manufactured copper

*Bradley D. Bock*¹, *Keagan Pretorius*¹ and *Seth. Scott*¹

¹Clean Energy Research Group, Department of Mechanical and Aeronautical Engineering, University of Pretoria, South Africa

Abstract. Recent technological advancements now allow for copper to be 3D printed, opening the doors for this technology to take a greater part in heat transfer applications. In this study, copper samples were additively manufactured through a print-debind-sinter process and thermally characterised in terms of thermal conductivity and specific heat capacity, and mechanically characterised in terms of Vickers hardness. The microstructure porosity levels appeared to control the thermal properties measured, with the thermal conductivity, while the specific heat was unaffected, while the heat treatment effect caused by the sintering process appeared to control the Vickers hardness measured.

1 Introduction

The 3D printing of copper and other high thermal conductivity metals using laser beam techniques struggles as a result of the heat of the laser beam rapidly being conducted away from the printing site, resulting in severe defects of the print [1]. High thermal conductivity materials are an important next step in 3D printing, as they will open the technology up to the field of heat transfer and as such a green laser based system has been developed to print copper [2], although these are typically prohibitively expensive proprietary technologies. Beamless 3D printing techniques have thus been investigated to solve this [1], with print-debind- sinter style methodologies having been developed as a typical cost effective answer to this problem.

There are a number of print-debind-sinter technologies used to produce more cost-effective 3D printing of metals than laser-based methods, each with variations on a standard methodology of suspending metal powder in a matrix that can be removed through a debinding step, before sintering the powder form to create a solid part. Chemical debinding processes use a solvent soluble matrix, such as a polyethylene glycol matrix that dissolves in water [3], so called “catalytic debinding” using gaseous nitric acid in a nitrogen atmosphere [4] or proprietary solvent [5]. Thermal debinding processes meanwhile use a high-temperature kiln to melt and sublimate the binder [6, 7].

The thermal sintering processes for the debinded metal powders also varies between manufacturers, with pure hydrogen or a vacuum required by some [4], while others submerge the part in sintering carbon to act as a sacrificial shield against oxidation [6].

Furthermore, many of these processes are fairly restrictive, with parts either being sent away to service providers to perform the debinding and sintering using proprietary

technologies [4] or require the purchase of multiple pieces of proprietary equipment if in-house processing is attempted [7]. Thus the user has little control over the process, which is not ideal for research purposes. This array of proprietary methods thus creates great uncertainty of the characteristics of the final printed parts and the process influences on them.

However, there are approaches that allow the user to control every step of the process [6]. The print-debind-sinter process itself can thus be varied, allowing for complete control to the user and so for research purposes, is a very powerful tool.

Characterisation of the specimens printed with these print-debind-sinter has begun to appear in literature, which have further highlighted how important process parameters such as sintering time, temperature and ballast can be on the final properties of the printed part. Dehdari Ebrahimi and Ju [8] showed that the thermal conductivity and Young's modulus of a copper printed specimen can vary between themselves by as much as a factor of 2, while the yield stress can vary by as much as a factor of 6, all as a result of variations made to the sintering process. Keraghel, et al. [9] found that hardness of bronze specimens varied by a factor of up to 2.5 due to changes in the sintering process. This wide range of characteristics thus shows the need to individually test samples to determine the characteristics that can be expected from any particular process, especially as these processes are still new and often in development.

For those processes where the sintering takes place in a sintering carbon and talc ballast in order to prevent sample oxidation and provide sample support [6] (rather than an inert atmosphere), no mention has been made in the literature of the effect the ballast has on the sintering process, such as the rate of inclusion of ballast as impurities within the sintered sample and the resulting effect on thermal and strength properties.

In this paper, the Vickers hardness, thermal conductivity and specific heat will be experimentally measured of debind-and-sinter 3D printed copper samples to determine their particular characteristics. This will serve as a first step in using 3D printed copper in heat transfer applications for future studies.

2 Methodology

2.1 Copper filament used

The copper filament used is approximately 90 % by weight copper powder, and 10 % by weight PLA, leading to a final density of the filament to be between 4500 to 4700 kg/m³ [10]. As the density of copper and PLA are estimated as 8940 kg/m³ [11] and 1240 kg/m³ [12] respectively, this equates to a volume fraction of the copper of approximately 40 %.

2.2 3D printing process

2.2.1 Printing process

The samples are printed using a Fused Filament Fabrication (FFF) style 3D printer, where filament composed of copper powder and a polymer matrix (PLA) are extruded to produce the part.

The only modifications needed to a standard desktop style printer (Ender 5 Plus) was a 0.6 mm hardened steel nozzle to ensure the metal particles within the filament did not wear the standard brass nozzle away, and a "filawarmer", which is a tube heater that the filament is fed through and heats the filament to 60°C to allow for sufficient flexibility of the filament to prevent breakages as it enters the printer feeder [6].

2.2.2 Debinding and sintering process

The green 3D printed samples were thermally debinded and sintered to produce the final sintered part.

The debinding process involves placing the green 3D printed part under a mixture of aluminium oxide (Al_2O_3) refractory and sintering carbon within a closed crucible which is then placed in a kiln. The purpose of the refractory is to provide mechanical support to the part as the PLA is removed during the debinding process. The kiln had a setpoint of $482^\circ C$ with a ramp rate of $55^\circ C/hr$, as per the manufacturers instruction [6].

The sintering process involves removing the refractory and replacing it with sintering carbon. This carbon acts as a sacrificial shield to prevent oxidation from atmospheric oxygen present in the kiln. The kiln is then set to $1052^\circ C$ with a ramp rate of $111^\circ C$ per hour [6]. Once the setpoint is reached, the kiln is held at $1052^\circ C$ for 5 hours. As this is close to the melting point of copper, the kiln must have sufficient control capabilities to not significantly ramp over the setpoint and reach the melting point at $1085^\circ C$. It should be noted that if excess oxygen gains access to the part and overwhelms the sintering carbon, severe oxidation can occur to the point of part failure.

Once sintering was complete, the kiln door was opened, and the part was allowed to air cool. The part was then removed, and the sintering carbon was cleaned off with a cloth.

2.3 Samples

Two solid copper reference samples of different grades were produced to test together with the sintered samples to validate the test equipment. The grades of copper were both 99.9 % pure copper, with hardened CDA 110 copper [13] and half hard C120 copper [14] used.

Two samples produced with the print-debind-sinter process were used.

2.4 Vickers hardness measurement

The Vickers hardness measurements were conducted with Future-Tec FM-700 microhardness tester, a fully digital tester where a diamond tipped point was pressed into the sample and the indentation dimensions measured via microscopic inspection through a screen readout, as per ISO 6507-1:2018 [15].

2.5 Thermal conductivity measurement

The thermal conductivity was measured using a steady state divided bar method, as illustrated in **Fig. 1**. A constant heat flux was applied to the top of the sample through a heating element supplying heat to a heated section, and a heat sink in the form of a cooling section was used beneath the sample to remove the heat applied. The thermal stack was insulated, and the temperature gradient was measured, allowing for the determination of the thermal conductivity of the sample piece. Further details on this measurement can be found in [16].

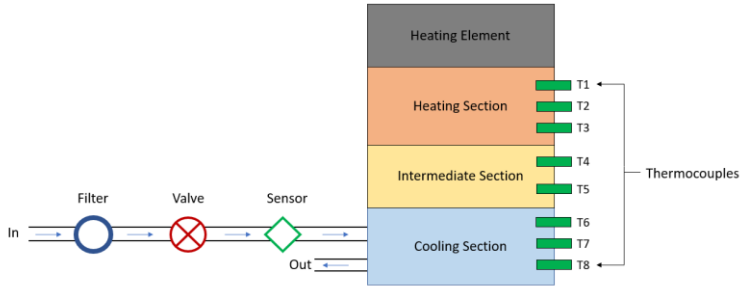


Fig. 1. Schematic illustration of the divided bar apparatus for the thermal conductivity tests

2.6 Specific heat capacity measurement

The specific heat capacity was measured using a bomb calorimeter. The test sample was heated to 96°C in boiling water, and then placed into the insulated bomb calorimeter, which was at room temperature. The temperature was recorded as the calorimeter came to thermal stabilisation, and the final temperature was used to calculate the specific heat capacity of the sample.

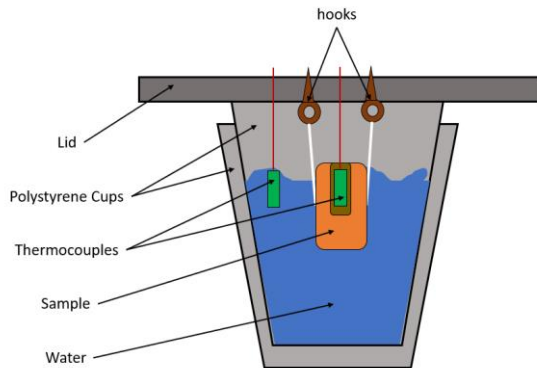


Fig. 2. Schematic illustration of the bomb calorimeter used for the specific heat capacity tests.

2.7 Porosity measurement

The porosity (ϵ) of the sintered samples was calculated as follows

$$\epsilon = 1 - \frac{\rho_{sintered}}{\rho_{reference}} \quad (1)$$

Where the density of the reference ($\rho_{reference}$) and sintered samples ($\rho_{sintered}$) were calculated from the measured mass and volume of the samples.

2.8 Modelled results

The thermal conductivity of the sintered part was calculated using the Aivazov and Domashnev [17] model, developed to predict the conductivity of porous specimens. The model takes the form of

$$\frac{k_{porous}}{k_m} = 1 - \frac{1-\epsilon}{1+11\epsilon^2} \quad (2)$$

Where k_{porous} is the effective thermal conductivity of the porous specimen, k_m is the thermal conductivity of the matrix and ϵ is the porosity.

3 Results

3.1 Porosity

The fully sintered samples in this study displayed porosity, as illustrated in Fig. 3. The unsintered PLA/copper sample, illustrated in Fig. 3 (a), clearly illustrates the composite mix of the sample, with a PLA matrix (the dark area of the image), which is about 60 % by volume of the composite, impregnated by copper powder (the bright spots of the image highlighted by black arrows).

The sintered sample, illustrated in Fig. 3 (b), shows clear porosity with numerous voids. The print-debind process introduces porosity into the parts, with the printing process not always able to lay down beads of material close enough to each other to prevent air gaps, as well as through the debinding process, where the removal of the PLA from the copper-PLA composite leaves voids in the remaining solid, creating a porous structure. The voids in Fig. 3 (b) appear relatively evenly distributed across the cross-section of the sample and no clear clumping of voids are visible.

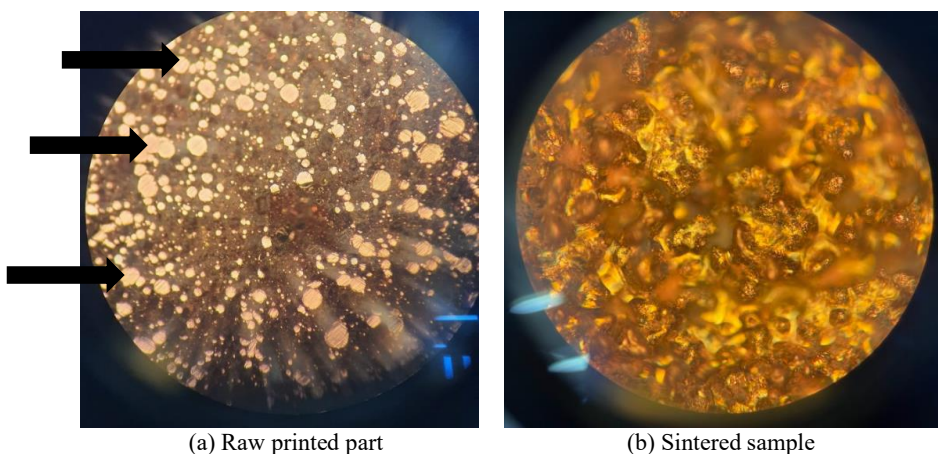


Fig. 3. Microscopic images of raw and sintered sample

Based on density and volume measurements, porosity of between 20 and 27% for the samples were calculated. Thus, while the PLA occupies a volume of about 60 % of the sample, the porosity is approximately half of that value for the sintering conditions used in this study.

It is well established that the subsequent sintering process is able to influence the porosity of sintered parts [9, 18], with the sintering time and temperature in particular easily adjustable

parameters that can control the porosity to some extent. For example, Dehdari Ebrahimi and Ju [8] found a porosity of 55 % for their study, despite using the exact same filament, but different sintering conditions. The magnitude of porosity reduction had been shown for other sintered powders to approach 0% [19], but this has not been confirmed for this copper-PLA print-debind-sinter process. No such effort to reduce porosity was made in this study, with parts sintered for the default amount of time as per the procedure outlined previously in section 2.2.

3.2 Vickers Hardness

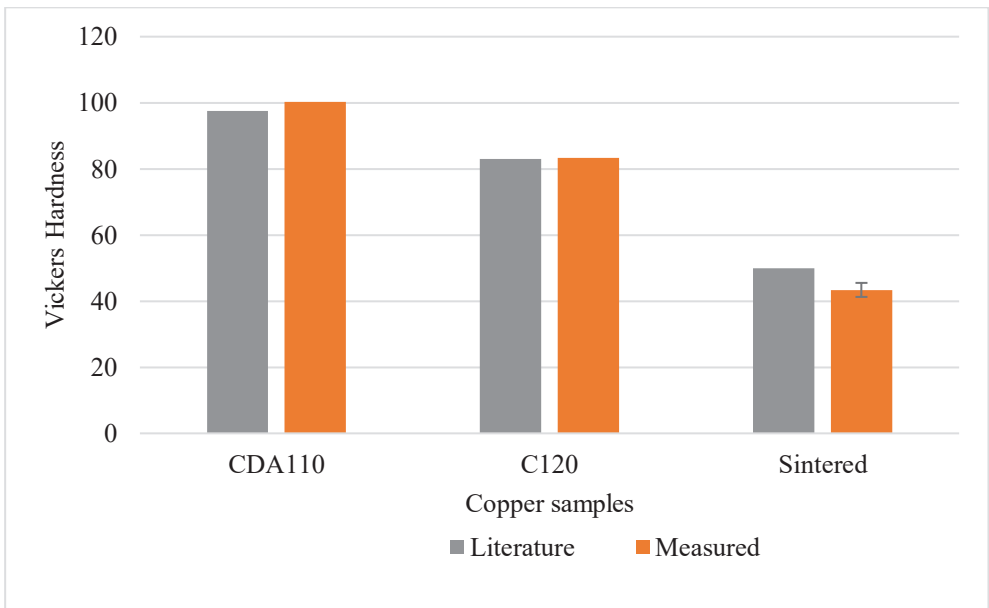


Fig. 4. Vickers hardness results

The Vickers hardness test results of the CDA 110, C120 reference samples and the sintered copper samples are illustrated in Fig. 4, with the standard deviation of the sintered sample measurements displayed as an error bar. Vickers hardness values in literature range between 90 and 105 for hardened CDA 110 [11], matching well with the measured value of 100. The grade C120 reference sample compares well with literature as well, and as it was a “half hard” annealed sample, it thus had a lower Vickers hardness than the CDA 110, and it is typically quoted as having a Vickers hardness of between 75 to 90 [11], which compared well with the measured Vickers hardness of 83.

The sintered copper had an average measured Vickers hardness of 43, less than half that of the reference copper samples. This compares closely with the Vickers hardness value of 50 supplied by the manufacturer [20], as well as the hardness’s of annealed coppers, with values of 50 [21] and 57 [22] found in literature. Thus, the hardness difference can largely be attributed to the heat treatment process the sintered copper powder undergoes during the cooling process after the completion of sintering, with the samples air cooled in this study, as noted in section 2.2.2, by allowing the kiln to cool with the door of the kiln open. This suggests that in future the final hardness of the part can be significantly influenced by the

cooling process used once the sintering is complete, similarly noted by Ayeni [23] in their study of the hardness of bronze 3D printed parts.

3.3 Specific Heat

The specific heats measured and modelled in the study are illustrated in Fig. 5. The reference C120 copper sample had a measured specific heat of 0.35 J/kgK, which compares well with the expected value of 0.385 J/kgK [14]. The sintered copper sample had an average specific heat of 0.37 J/kgK, which is within 3 % of the reference copper sample. Thus, the print-debind-sinter process had largely unchanged this thermal property. This suggests that the possible inclusion of impurities from the process, namely the Al_2O_3 debinding ballast or sintering carbon, has not occurred to any significant extent.

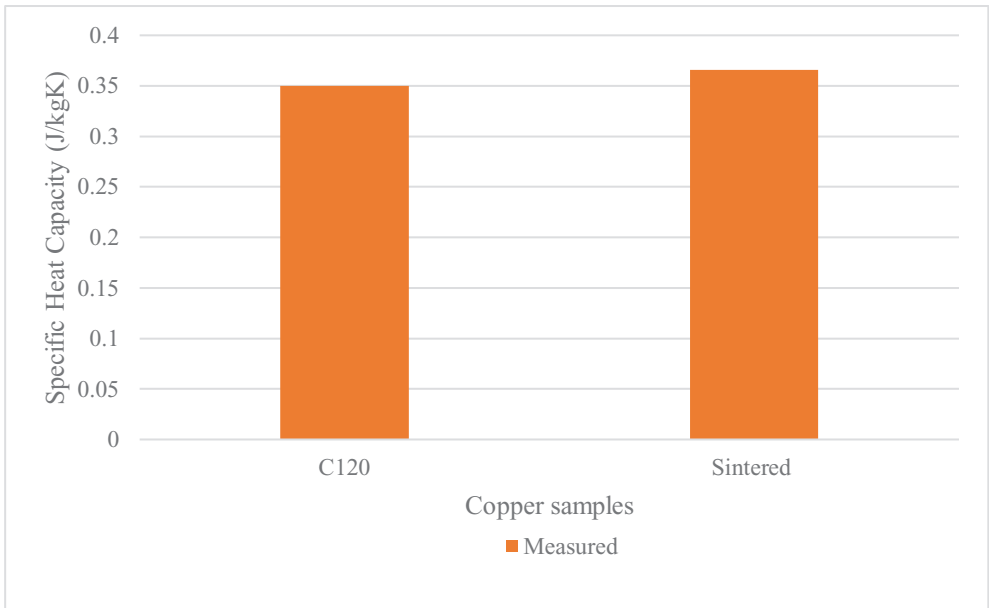


Fig. 5. Specific heat capacity results

3.4 Thermal conductivity

The thermal conductivities measured and modelled for the reference and sintered copper samples are shown in **Fig. 6**, with the standard deviation of the measured sinter samples shown as an error bar.

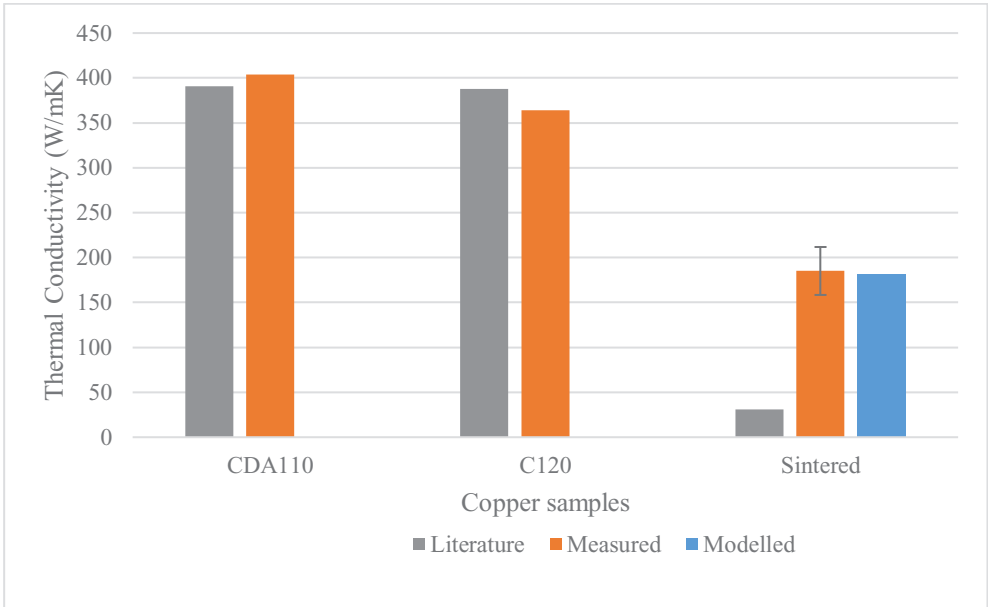


Fig. 6. Thermal conductivity results

The reference copper samples measured 404 and 364 W/mK, as compared to the typically quoted literature values of 391 [11] and 388 W/mK [14]. A maximum deviation of 7% was thus found between the C120 measured and literature values, which was considered satisfactory agreement.

The sintered samples measured on average a thermal conductivity of 185 W/mK, which is approximately 50 % of the reference samples. Considering that the specific heats measured of the sintered samples were very close to that of the reference samples, it appears insignificant inclusions and impurities are present in the sintered copper samples. Instead, the porosity of the sintered copper samples is thought to be the major influence behind these differences in thermal conductivity.

Aivazov and Domashnev [17] predicted an average thermal conductivity of 181 W/mK using the calculated porosities for each sintered sample, which is within 10 % of the measured thermal conductivities. These modelled results used a model specifically developed to factor in the influence of porosity on the thermal conductivity of a specimen thus further support the idea that the lower thermal conductivity can largely be attributed to the porosity. Considering that porosity is thus considered the driving factor behind the thermal conductivity reduction, this bulk thermal conductivity should be able to be modified through the variation of the sintering process parameters, which will vary the porosity produced [9, 18].

4 Conclusion

The porosity, Vickers hardness, thermal conductivity and specific heat capacity of copper samples printed with a debind-and-sinter style 3D printing process were experimentally measured and mathematically modelled, as well as reference copper samples for validation's sake.

The porosity of the sintered samples was found to be between 20 and 27 %. This porosity can be adjusted in future tests through varying sintering parameters such as sintering time or temperature.

The Vickers hardness of the sintered samples was found to be on average 43, which is less than half of the 100 of the copper particles used to print the part. This reduction in hardness is likely due to the annealing taking place as the part cools in the kiln and can thus be modified if different cooling processes were used.

The specific heat of the sintered samples was measured as 0.366 J/kgK, which was within 3 % of the reference copper samples. Thus, the 3D printing had no significant effect on this property. This thus suggests that no significant inclusions or impurities were noted within the sintered sample as a result of the debinding or sintering process, where the part was submerged in mixtures of aluminium oxide and sintering carbon.

The average thermal conductivity measured was approximately 185 W/mK, about half that of the reference copper samples measured in this study. This reduction in thermal conductivity was largely attributed to the porosity of the sintered sample.

The thermal conductivity of the 3D printed sample was about 50 % of a respective reference copper sample, and the porosity of the samples is considered the primary cause of the reduction in thermal conductivity. This could be increased in future if the sintering time is increased so that the porosity is decreased towards zero.

References

1. G. Singh and P. M. Pandey, "Experimental investigations into mechanical and thermal properties of rapid manufactured copper parts," *Proceedings of the Institution of Mechanical Engineers, Part C: Journal of Mechanical Engineering Science*, vol. 234, no. 1, pp. 82-95, 2020, doi: 10.1177/0954406219875483.
2. Trumpf. "Green laser: 3D printing of copper and copper alloys." https://www.trumpf.com/en_INT/products/machines-systems/additive-production-systems/truprint-5000-green-edition/ (accessed).
3. G. Singh, J.-M. Missiaen, D. Bouvard, and J.-M. Chaix, "Copper additive manufacturing using MIM feedstock: adjustment of printing, debinding, and sintering parameters for processing dense and defectless parts," *The International Journal of Advanced Manufacturing Technology*, vol. 115, no. 1, pp. 449-462, 2021/07/01 2021, doi: 10.1007/s00170-021-07188-y.
4. Basf, "Ultrafuse® Metal Filaments." [Online]. Available: https://move.forward-am.com/hubfs/AES%20Documentation/Metal%20Filaments/Ultrafuse_metal_Use_r_Guideline.pdf
5. Markforged. "Markforged Metal 3D Printer: The Metal X 3D Printing System." <https://markforged.com/3d-printers/metal-x> (accessed).
6. Virtual Foundry. "Printing pure metal with Filamet™." @virtualfoundry. <https://thevirtualfoundry.com/help/> (accessed).
7. D. Metal. "Studio System™." @DesktopMetal. <https://www.desktopmetal.com/products/studio> (accessed).
8. N. Dehdari Ebrahimi and Y. S. Ju, "Thermal conductivity of sintered copper samples prepared using 3D printing-compatible polymer composite filaments," *Additive Manufacturing*, vol. 24, pp. 479-485, 2018/12/01/ 2018, doi: <https://doi.org/10.1016/j.addma.2018.10.025>.
9. F. Keraghel, k. Loucif, and M. P. Delplancke, "STUDY OF BRONZE POROUS ALLOY Cu-Sn WORKED OUT BY METALLUGY OF THE POWDERS," *Physics Procedia*, vol. 21, pp. 152-158, 2011/01/01/ 2011, doi: <https://doi.org/10.1016/j.phpro.2011.10.023>.

10. Virtual Foundry, "Safety Datasheet - Copper Filamet." [Online]. Available: <https://thevirtualfoundry.com/wp-content/uploads/2021/12/The-Virtual-Foundry-SDS-Copper-21-12.pdf>
11. Mitsubishi. "Alloy Guide - Strip and Plate." https://www.mitsubishi-copper.com/en/assets/pdf/AlloyGUIDE_EN.pdf (accessed).
12. W. i. t. d. o. P. L. A. f. plastic. "All About the Density of PLA." @all3dp. <https://all3dp.com/2/pla-density-what-s-the-density-of-pla-filament-plastic/> (accessed).
13. MatWeb. "Electrolytic Tough Pitch (ETP) Copper, UNS C11000, OSO50 Temper flat products, rod, tube, shapes." <https://www.matweb.com/search/DataSheet.aspx?MatGUID=41a3ab3af15a4ca7b8d558b974d8eb51> (accessed 2023/06/02).
14. MatWeb. "Copper, UNS C12000." <https://www.matweb.com/search/datasheet.aspx?matguid=91c2b0cb8af748dfb7367bb59e1fc9b8> (accessed 2023/0623, 2023).
15. E. DIN, "6507-1 (2018.): Metallic materials-Vickers hardness test-Part 1: Test method (ISO 6507-1: 2018)," *European committee for standardization, CEN-CENELEC, Brussels, Belgium*, 2018.
16. D. Zhao, X. Qian, X. Gu, S. A. Jajja, and R. Yang, "Measurement Techniques for Thermal Conductivity and Interfacial Thermal Conductance of Bulk and Thin Film Materials," *Journal of Electronic Packaging*, vol. 138, no. 4, 2016, doi: 10.1115/1.4034605.
17. M. I. Aivazov and I. A. Domashnev, "Influence of porosity on the conductivity of hot-pressed titanium-nitride specimens," *Soviet Powder Metallurgy and Metal Ceramics*, vol. 7, no. 9, pp. 708-710, 1968/09/01 1968, doi: 10.1007/BF00773737.
18. M. A. Almomani, A. M. Shatnawi, and M. K. Alrashdan, "Effect of Sintering Time on the Density, Porosity Content and Microstructure of Copper – 1 wt. % Silicon Carbide Composites," *Advanced Materials Research*, vol. 1064, pp. 32-37, 2015, doi: 10.4028/www.scientific.net/AMR.1064.32.
19. R. M. German, P. Suri, and S. J. Park, "Review: liquid phase sintering," *Journal of Materials Science*, vol. 44, no. 1, pp. 1-39, 2009/01/01 2009, doi: 10.1007/s10853-008-3008-0.
20. Virtual Foundry, "Technical Data Sheet - Copper Filamet." [Online]. Available: <https://thevirtualfoundry.com/wp-content/uploads/2022/11/The-Virtual-Foundry-TDS-Copper-22-11.pdf>
21. MatWeb. "Copper, Cu; Annealed." https://www.matweb.com/search/datasheet_print.aspx?matguid=9aeb83845c04c1db5126fada6f76f7e (accessed 2023/06/02).
22. J. Yu, G. Wang, and Y. Rong, "Experimental Study on the Surface Integrity and Chip Formation in the Micro Cutting Process," *Procedia Manufacturing*, vol. 1, pp. 655-662, 2015/01/01/ 2015, doi: <https://doi.org/10.1016/j.promfg.2015.09.063>.
23. O. Ayeni, "Sintering and Characterizations of 3D Printed Bronze Metal Filament," Purdue University Graduate School, 2019.